J. Fluid Mech. (1991), *vol.* 222, *pp.* 39–60
Printed in Great Britain

The axial flow of a Bingham plastic in a narrow eccentric annulus

By I. C. WALTON AND S. H. BITTLESTON
Schlumberger Cambridge Research, Madingley Road, Cambridge CB3 0EL, UK

(Received 15 July 1989 and in revised form 23 April 1990)

This paper describes analytical and numerical solutions for the flow of a Bingham plastic in an eccentric annulus. Analytical solutions are obtained by expanding in powers of δ, the ratio of the difference in radii of the bounding cylinders to their mean. The solution over most of the annulus is similar to that in a slot of uniform width, containing a central plug-like region over which the velocity is independent of the radial variable. However, unlike the uniform-slot solution, the velocity in the plug varies around the annulus and the stress exceeds the yield stress. This simple structure is supplemented by true plugs (over which the velocity is constant and the stress is below the yield stress) at the widest and, in some cases, the narrowest parts of the annulus. A simple criterion is given for conditions under which the fluid ceases to flow on the narrow side and bounds are obtained for the extent of the motionless region and for the true plugs.

The predictions of the theory have been compared to numerical results over a wide range of eccentricities, radius ratios, fluid properties and flow parameters. Good quantitative agreement has been reached for radius ratios in excess of about 0.7. In particular the extent and location of pseudo-plugs and true plugs are confirmed.

1. Introduction

Many fluids commonly used in industry have rheologies very different from that of Newtonian fluids. In particular, many pastes and suspensions exhibit shear-thinning behaviour and in addition possess a yield stress below which the fluid either will not flow or will flow as an unsheared plug. The simplest yield-stress fluid is a Bingham plastic for which the stress–rate of strain relation is linear above the yield stress. Many industrial applications of the Bingham rheology are described in a review by Bird, Dia & Yarusso (1983).

Bird *et al.* (1983) have also reviewed all known exact solutions for the flow of Bingham plastics in simple geometries (including a slot and a concentric annulus). A common feature of all the flows described in that review is an unsheared plug whose boundaries are parallel to the physical boundaries. Relatively little is known about the flow of yield-stress fluids in more complex geometries in which the physical boundaries are not parallel, or more generally, in which the cross-sectional area is not uniform. A fundamental difficulty in numerical and analytic procedures is to determine the location of the yield surfaces. Indeed, there is some dispute in the literature about whether such regions of unsheared flow can really exist in complex geometries.

Lipscombe & Denn (1984) argued that while shear-free regions may sometimes be approximated, yielding and flow must occur everywhere in complex geometries.

These conclusions were developed in the context of pressure-driven flow between divergent planes and applied specifically to squeeze-film flow and the radial flow between stationary discs. The results of our own investigation lend some qualified support to this view, but we do not rule out the possibility of plugs of limited extent existing in some complex geometries. Gartling & Phan-Thien (1984) developed numerical and analytic results for the squeeze-film problem for a biviscosity plastic fluid, of which a Bingham plastic may be regarded as a limiting case. They claimed that a yield surface does exist even though their velocity profiles were very similar to Lipscombe & Denn's and clearly exhibited elongational shear. There is no real disagreement between the results presented in these papers, only in their interpretation. The situation has been clarified by O'Donovan & Tanner (1984) who undertook careful numerical calculations of this problem. They showed that in the regions that appear to be plugs the stress exceeds the yield stress but only by a very small amount. A novel and complicating feature of their results is the presence of small unyielded regions near the centres of the discs. Numerical results have been obtained by Beris *et al.* (1985) for slow flow of a Bingham plastic round a sphere. Their calculations indicate the presence of unyielded regions at the poles of the sphere and at large distances from the sphere. There is as yet no published analytic evidence for the existence of unyielded regions in complex geometries and the definitive solutions are still awaited. However, there is an extensive literature concerning the existence of unyielded regions in rigid/plastic solids (see Hill 1950), which may be regarded as a limiting case of a Bingham plastic as the plastic viscosity tends to zero. For example, Beris *et al.* (1985) were able to demonstrate that the limiting case of their solution for the outer yield surface was well approximated by the corresponding results for rigid/plastic solids. Such results support the view that unyielded regions can exist for Bingham plastics even in complex geometries.

The present work considers the axial flow of a Bingham plastic in a narrow eccentric annulus and has two main motivations. First, it seeks to model the flow of pastes and suspensions in a complex geometry that has industrial applications. Second, by solving the problem numerically and analytically, using perturbation techniques, we attempt to arrive at a definitive conclusion about the nature of the stress distribution and the location of any yield surfaces. There is a large body of published work, both theoretical and experimental, on the flow of Newtonian fluids through eccentric annuli (see, for example, Snyder & Goldstein 1965), but there is relatively little in the literature on the flow of non-Newtonian fluids in such a geometry. Mitsuishi & Aoyagi (1973) presented experimental and numerical results (using a variational technique) for the flow of a Sutterby fluid, while Iyoho & Azar (1980) used a narrow-gap approximation to obtain results for power-law fluids. Guckes (1975) obtained numerical results for power-law fluids and Bingham plastics but only over a limited region of parameter space. There seems to be no published solution for the corresponding problem involving a rigid/plastic solid.

The plan of the paper is as follows. The problem and the rheology are defined in §2, and the analytic solution for small annular gaps is obtained in §3. The procedure for obtaining numerical solutions is described in §4. Finally, in §5, the analytic and numerical results are described and compared and some conclusions are drawn about the nature of the yield surface and the plug regions.

2. Governing equations

The simplest rheological model of a fluid that exhibits a yield stress is the Bingham plastic whose constituative equation can be written

$$\boldsymbol{\tau}^* = \mu^* \dot{\boldsymbol{\gamma}}^* \quad \text{for } \tau^* > \tau_y^*, \tag{1}$$

$$\dot{\boldsymbol{\gamma}}^* = 0 \quad \text{for } \tau^* \leqslant \tau_y^*, \tag{2}$$

where the viscosity, μ^*, is defined by

$$\mu^* = \mu_0^* + \frac{\tau_y^*}{\dot{\gamma}^*} \tag{3}$$

and $\boldsymbol{\tau}^*$ is the stress tensor, $\dot{\boldsymbol{\gamma}}^*$ is the rate-of-strain tensor, τ_y^* the yield stress and μ_0^* the plastic viscosity. The second invariants of the stress and rate-of-strain tensors are defined by

$$\tau^* = [\tfrac{1}{2}(\boldsymbol{\tau}^* : \boldsymbol{\tau}^*)]^{\frac{1}{2}}, \tag{4}$$

$$\dot{\gamma}^* = [\tfrac{1}{2}(\dot{\boldsymbol{\gamma}}^* : \dot{\boldsymbol{\gamma}}^*)]^{\frac{1}{2}}. \tag{5}$$

The surface $\tau^* = \tau_y^*$ marks the boundary between shearing fluid and fluid that is either at rest or moving with a uniform velocity. The location of this surface (or surfaces) is not known *a priori* and presents one of the major difficulties in obtaining numerical solutions. An additional difficulty in obtaining numerical results is the singularity in (3) as $\dot{\gamma}^* \to 0$, i.e. as the yield surface is approached. We follow the approach adopted by several authors (notably Bercovier & Engleman (1980) and Beris *et al.* (1985)) in replacing $\dot{\gamma}^*$ with $\dot{\gamma}^* + \epsilon$ in (3), where ϵ is a small parameter (typically $O(10^{-8})$). It is not necessary to resort to this device in order to obtain analytic solutions, but unless a sub-yield-stress model is specified the stress field within any yield surfaces cannot be calculated.

The fully developed velocity field for axial flow arises through a balance between viscous forces and the pressure gradient. The equation of conservation of momentum is

$$\frac{\mathrm{d}p^*}{\mathrm{d}z^*} = \boldsymbol{\nabla}^* \cdot \boldsymbol{\tau}^*, \tag{6}$$

where p^* is the dynamic pressure and z^* is measured axially in the direction of flow. For an incompressible fluid the axial velocity component, w^*, is independent of z^*.

It is convenient to non-dimensionalize the governing equations with reference to a velocity scale, w_0^*, and a lengthscale, d^*, which is taken to be the difference in the radii of the two bounding cylinders. We define a dimensionless radial coordinate, x, by writing

$$r^* = r_I^*(1 + \delta x), \tag{7}$$

where $\delta = d^*/r_I^*$ is a dimensionless gap width.

The viscosity is scaled on μ_0^* and the stress on $\mu_0^* w_0^*/d^*$. Equations (1), (2) become

$$\boldsymbol{\tau} = \mu \dot{\boldsymbol{\gamma}} \quad \text{for } \tau > Bn, \tag{8}$$

$$\dot{\boldsymbol{\gamma}} = 0 \quad \text{for } \tau \leqslant Bn, \tag{9}$$

where

$$\mu = 1 + \frac{Bn}{\dot{\gamma}} \tag{10}$$

and

$$Bn = \frac{\tau_y^* d^*}{\mu_0^* w_0^*} \tag{11}$$

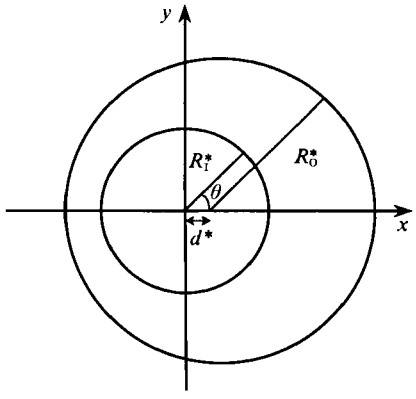

FIGURE 1. Annular geometry and coordinate system.

is called the Bingham number. The momentum equation becomes

$$\nabla\cdot\boldsymbol{\tau} = -P, \tag{12}$$

where

$$P = -\frac{d^{*2}\,\mathrm{d}p^*/\mathrm{d}z^*}{\mu_0^*\, w_0^*} \tag{13}$$

is the dimensionless pressure gradient. Solutions will be obtained for constant pressure gradient, in which case w_0^* is defined by $w_0^* = d^{*2}(-\mathrm{d}p^*/\mathrm{d}z^*)/\mu_0^*$ so that

$$P = 1 \quad \text{and} \quad Bn = \tau_y^*/d^*(-\mathrm{d}p^*/\mathrm{d}z^*). \tag{14}$$

Alternatively, if the flow rate, Q^*, is specified then $w_0^* = Q^*/A^*$, where A^* is the cross-sectional area, P remains unspecified, but w is now subject to the additional constraint

$$\iint w\,\mathrm{d}\Omega = 1, \tag{15}$$

where $\mathrm{d}\Omega$ is an element of the cross-sectional area.

The geometry of the eccentric annulus is shown in figure 1. The circular boundaries are defined by

$$C_\mathrm{I}: \quad x_1^{*2} + x_2^{*2} = r_\mathrm{I}^{*2}, \tag{16}$$

$$C_\mathrm{O}: \quad (x_1^* - e^*)^2 + x_2^{*2} = r_\mathrm{O}^{*2}, \tag{17}$$

where $r_\mathrm{I}^*, r_\mathrm{O}^*$ are the radii of the inner and outer cylinders respectively and e^* is the offset of their centres.

The boundary conditions appropriate for non-slip boundaries are

$$w = 0 \quad \text{on} \quad C_\mathrm{I} \quad \text{and} \quad C_\mathrm{O}. \tag{18}$$

At the yield surfaces both the velocity and the stress fields are required to be continuous.

3. The narrow-gap approximation

The analysis which follows is based on the simplifying approximation that the gap between the two cylinders is everywhere small compared with the mean radius. It is equivalent, at least to a first approximation, to neglecting the effect of curvature and treating the annulus as if it were a slot of variable width, this variation taking place on a lengthscale much larger than the mean slot width.

In terms of the scaled radial variable, x, and an angle θ measured anticlockwise from the widest part of the annulus (see figure 1), the boundaries are located at $x = 0, h(\theta)$ defined by

$$\delta^2 h^2 + 2\delta h - 2\delta(1+\delta h)\, e\cos\theta = 2\delta + \delta^2(1-e^2). \tag{19}$$

Here e varies between 0 for a concentric annulus and 1 if the cylinders are in contact with one another. The narrow-gap approximation consists in letting $\delta \to 0$, while e remains $O(1)$. Under these conditions an approximate solution for h can now be found by expanding in powers of δ, i.e.

$$h = h_0 + \delta h_1 + O(\delta^2). \tag{20}$$

It can easily be deduced from (19) that

$$h_0 = 1 + e\cos\theta. \tag{21}$$

To leading order in δ the maximum and minimum dimensionless gap widths are

$$h_0(0) = 1+\epsilon, \quad h_0(\pi) = 1-\epsilon, \tag{22}$$

respectively. In terms of these new coordinates, (12) becomes

$$\frac{\partial \tau_{xz}}{\partial x} + \delta(1+\delta x)^{-1}\left(\frac{\partial \tau_{\theta z}}{\partial \theta} + \tau_{xz}\right) = -P, \tag{23}$$

where

$$\tau_{xz} = \mu\dot{\gamma}_{xz}, \tag{24}$$

$$\tau_{\theta z} = \mu\dot{\gamma}_{\theta z}, \tag{25}$$

$$\dot{\gamma}_{xz} = \frac{\partial w}{\partial x}, \tag{26}$$

$$\dot{\gamma}_{\theta z} = \delta(1+\delta x)^{-1}\frac{\partial w}{\partial \theta}, \tag{27}$$

$$\dot{\gamma} = [\dot{\gamma}_{xz}^2 + \dot{\gamma}_{\theta z}^2]^{\frac{1}{2}}. \tag{28}$$

For $\delta \ll 1$ it is natural to seek a solution by expanding in powers of δ. Thus, if w is expanded as

$$w = w_0 + \delta w_1 + O(\delta^2), \tag{29}$$

then it follows that the components of the rate-of-strain tensors take the form

$$\dot{\gamma}_{xz} = \dot{\gamma}_{xz0} + \delta\dot{\gamma}_{xz1} + O(\delta^2), \tag{30}$$

$$\dot{\gamma}_{\theta z} = \delta\dot{\gamma}_{\theta z1} + O(\delta^2), \tag{31}$$

where

$$\dot{\gamma}_{xz0} = \frac{\partial w_0}{\partial x}, \quad \dot{\gamma}_{xz1} = \frac{\partial w_1}{\partial x}, \quad \dot{\gamma}_{\theta z1} = \frac{\partial w_0}{\partial \theta}. \tag{32}$$

The components of the stress tensor are also expanded in powers of δ as follows:

$$\tau_{xz} = \tau_{xz0} + \delta\tau_{xz1} + O(\delta^2), \tag{33}$$

$$\tau_{\theta z} = \delta\tau_{\theta z1} + O(\delta^2). \tag{34}$$

3.1. *The leading-order solution*

Having set up all the relevant expansions, the next step is to substitute them into the governing equations and equate coefficients of powers of δ to zero. This process is, in principle, quite straightforward, but in practice is complicated by the necessity

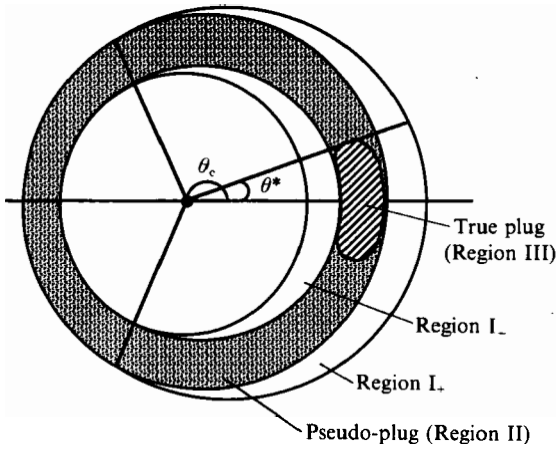

FIGURE 2. Flow regions in the annulus.

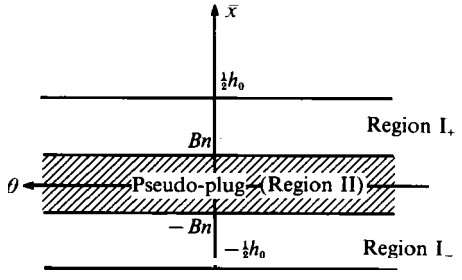

FIGURE 3. Flow regions in the central section of the annulus.

to divide the annulus into a number of regions in each of which a different form of solution must be found. For simplicity of presentation we shall restrict the following discussion to the constant-pressure-gradient case and set $P = 1$. As explained in §2 there is no loss in generality in so doing, since this choice merely reflects the chosen scaling for the velocity field. The constant-flow-rate case is similar but involves an extra iteration on P to satisfy the constraint, (15). The leading-order solution is obtained by substituting the expansions into the governing equations and retaining only the largest terms. Thus, the leading terms in (23) give

$$\frac{\partial}{\partial x}\tau_{xz0} = -1. \tag{35}$$

On integration and after appealing to symmetry about $x = 0$ this gives

$$\tau_{xz0} = -\bar{x}, \tag{36}$$

where $\bar{x} = x - \frac{1}{2}h_0$. Since the yield surfaces are now defined by $\tau = \pm Bn$, it follows that they are located at $\bar{x} = \mp Bn$. The region within these surfaces will be designated Region II and the regions outside will be denoted by Regions $\mathrm{I}_\pm$ for $\bar{x} > Bn$ and $\bar{x} < -Bn$, respectively, as shown in figures 2, 3. In Regions $\mathrm{I}_\pm$ equation (8) applies; to leading order it gives

$$\dot{\gamma}_{xz0} + \mathrm{sgn}\,(\dot{\gamma}_{xz0})\,Bn = -\bar{x}, \tag{37}$$

i.e. $$\dot{\gamma}_{xz0} = -(\bar{x} \pm Bn). \tag{38}$$

The solution that satisfies the no-slip boundary conditions

$$w_0 = 0 \quad \text{at} \quad \bar{x} = \pm \tfrac{1}{2} h_0 \tag{39}$$

is $$w_0 = -\tfrac{1}{2}[(\bar{x} \mp Bn)^2 - (\tfrac{1}{2}h_0 - Bn)^2]. \tag{40}$$

Inside the yield surfaces $\dot{\gamma}_{xz0} = 0$, from which it follows that w_0, does not change across this region and is equal to its value on the yield surfaces, i.e.

$$w_0 = w_{p0} = \tfrac{1}{2}(\tfrac{1}{2}h_0 - Bn)^2. \tag{41}$$

This solution represents a plug flow, moving with velocity w_{p0}, flanked by sheared regions between the yield surfaces and the walls. The thickness of the plug region is independent of θ and is in fact equal to $2Bn$. Provided that $2Bn$ is smaller than the minimum gap width, $(1-e)$, the plug extends all round the annulus. If, however, $2Bn$ exceeds this value then there is a critical angle, which will be denoted by θ_c, at which the plug begins to fill the gap. Using the first approximation to the gap width in (21) it can be seen that, to leading order, θ_c is given by

$$\theta_c = \cos^{-1}\left(\frac{2Bn-1}{e}\right). \tag{42}$$

Where the plug fills the gaps ($|\theta| > \theta_c$) the velocity of the fluid within the plug is zero, since it must satisfy the no-slip boundary conditions. This highlights the fact that the velocity within the plug is independent only of x; it does in fact vary with θ through its dependence on the gap width, h_0.

The solution as presented above is now seen to be incomplete, for on the one hand the stress has been assumed to lie below the yield stress in the plug regions while, on the other hand, the velocity there clearly varies with θ, which requires the stress to exceed the yield stress. It was a similar observation that led Lipscombe & Denn (1984) to conclude that plugs cannot exist unless the boundaries are parallel. If Region II is not a true plug, it is nevertheless plug-like and we shall therefore refer to the region within $\bar{x} = \pm Bn$ as the pseudo-plug and the surfaces $\bar{x} = \pm Bn$ as the pseudo-yield surfaces.

Outside the pseudo-yield surfaces the (x, z)-component of the stress tensor is $O(1)$ and is given by (36). The (θ, z)-component is only $O(\delta)$ and is given by

$$\tau_{\theta z1} = \left(1 + \frac{Bn}{|\dot{\gamma}_{xz0}|}\right)\frac{\partial w_0}{\partial \theta}, \tag{43}$$

with $\dot{\gamma}_{xz0}$ given in (38). Clearly, $\tau_{\theta z1}$ remains $O(1)$ as long as $|\dot{\gamma}_{xz0}|$ remains $O(1)$, but at the pseudo-yield surface $\dot{\gamma}_{xz0} = 0$ and this solution becomes singular.

3.2. *Solution in the pseudo-plug region*

The increase in magnitude of $\tau_{\theta z1}$ as the pseudo-yield surface is approached suggests that inside the pseudo-yield surface both components of the stress tensor (and hence of the rate-of-strain tensor) are of the same order of magnitude and that a solution should be sought by writing

$$w = w_p = w_{p0}(\theta) + \delta w_{p1}(\theta, x) + O(\delta^2). \tag{44}$$

Then
$$\dot{\gamma}_{xz} = \delta \frac{\partial w_{\mathrm{p1}}}{\partial x} + \ldots, \tag{45}$$

$$\dot{\gamma}_{\theta z} = \delta \frac{\mathrm{d}w_{\mathrm{p0}}}{\mathrm{d}\theta} + \ldots, \tag{46}$$

$$\dot{\gamma} = \delta \left[\left(\frac{\partial w_{\mathrm{p1}}}{\partial x} \right)^2 + \left(\frac{\mathrm{d}w_{\mathrm{p0}}}{\mathrm{d}\theta} \right)^2 \right]^{\frac{1}{2}} + \ldots, \tag{47}$$

$$= \delta \dot{\gamma}_1 + \ldots. \tag{48}$$

Equation (36) still holds for τ_{xz0}, but now the constitutive relation (equation (8)) gives

$$\tau_{xz0} = -\bar{x} = \frac{Bn}{\dot{\gamma}_1} \frac{\partial w_{\mathrm{p1}}}{\partial x}. \tag{49}$$

Straightforward integration yields

$$w_{\mathrm{p1}} = Bn \left(1 - \frac{\bar{x}^2}{Bn^2} \right)^{\frac{1}{2}} \left| \frac{\mathrm{d}w_{p0}}{d\theta} \right| + w^*_{\mathrm{p1}}(\theta). \tag{50}$$

Here $w^*_{\mathrm{p1}}(\theta)$ is obtained by matching with the second-order solution outside the pseudo-plug; details will not be given here since the result is not relevant to the further development of the theory.

The leading contribution to $\tau_{\theta z}$ is now $O(1)$ and is given by

$$\tau_{\theta z0} = \frac{Bn}{\dot{\gamma}_1} \frac{\mathrm{d}w_{\mathrm{p0}}}{\mathrm{d}\theta}. \tag{51}$$

Use of (47), (48) (50) to eliminate $\dot{\gamma}_1$ and $\partial w_{\mathrm{p1}}/\partial x$ gives

$$\tau_{\theta z0} = \operatorname{sgn}\left(\frac{\mathrm{d}w_{\mathrm{p0}}}{\mathrm{d}\theta} \right) Bn \left(1 - \frac{\bar{x}^2}{Bn^2} \right)^{\frac{1}{2}}. \tag{52}$$

There are three aspects of this solution that merit comment. First, $\tau_{\theta z0} \to 0$ as $\bar{x} \to \pm Bn$, which indicates that relatively high values of the (θ, z)-component of the stress tensor are confined to the pseudo-plug.† Second, the second invariant of the stress tensor is given by

$$\tau^2 = \tau^2_{xz0} + \tau^2_{\theta z0} + \ldots, \tag{53}$$

$$= Bn^2 + \ldots. \tag{54}$$

Thus, even within the pseudo-plug, the stress exceeds the yield stress and this accounts for the shear seen in the leading approximation to the axial velocity component there. It has already been demonstrated that this shear results from the boundaries being non-parallel and this argument would seem to support Lipscombe & Denn's contention and demolish any possibility of true sub-yield-stress plugs in

† More precisely, $\tau_{\theta z0} \sim |Bn \pm \bar{x}|^{\frac{1}{2}}$ as $\bar{x} \to \mp Bn$. Outside the yield surface $\tau_{\theta z0} \sim \delta/(Bn \pm \bar{x})$ as $\bar{x} \to \mp Bn$. The mis-match is smoothed out in regions of thickness $\delta^{\frac{2}{3}}$ centred at $\bar{x} = \pm Bn$. The solution is straightforward and details will not be given here.

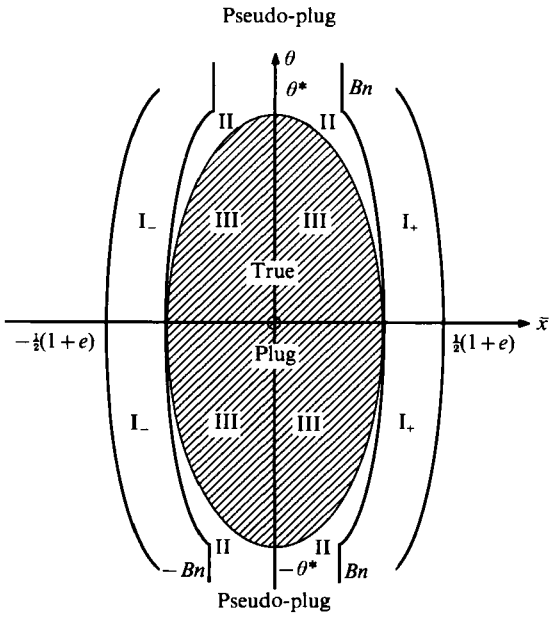

FIGURE 4. Flow regions near $\theta = 0$.

complex geometries. However, the solution even now is not complete. The third important feature of the pseudo-plug solution is that, since $\mathrm{d}w_{\mathrm{p0}}/\mathrm{d}\theta$ changes sign across $\theta = 0$ (and $\theta = \pi$, if the pseudo-plus extends that far), $\tau_{\theta z0}$ possesses a discontinuity there. A closer examination of the regions near $\theta = 0, \pi$ is required and it is here that true plugs appear.

3.3. *Solution near* $\theta = 0$

On the centreline of the annulus ($\bar{x} = 0$) $\tau_{xz} = 0$ and, at least to leading order, $\tau_{\theta z}$ takes the values $\pm Bn$ on opposite sides of $\theta = 0, \pi$. If regions exist close to $\theta = 0, \pi$ in which $\tau_{\theta z}$ changes smoothly from $+Bn$ to $-Bn$, then, at least near the centreline, $\tau^2 < Bn^2$ and a true plug exists.

In the solution given above it has been assumed that variations with θ take place on a much longer lengthscale than do variations with radial distance. Consequently, θ-variations appear only parametrically. A solution will now be sought in the regions near $\theta = 0, \pi$ on the basis that variations with θ take place on a smaller scale than before, but still larger than the scale of the radial variations, in such a way that derivatives with respect to θ appear at leading order. The proposed structure of the solution near $\theta = 0$ is shown in figure 4. Regions $\mathrm{I}_{\pm}$ lie outside the pseudo-plus as before and Region II is an extension of the pseudo-plug itself. There is now a new region, Region III, the true plug. It is bounded by $\theta = \pm\theta^*$, where it is expected that $\delta \ll \theta^* \ll 1$; a precise expression for θ^* will be determined below. Note that the pseudo-plug has been widened to accommodate the true plug and that relative to the centreline of the annulus, $\bar{x} = 0$, both cylindrical boundaries appear to be concave.

By definition, the velocity within the true plug is constant; it must therefore be equal to the velocity on the centreline of the annulus at $\theta = \pm\theta^*$. From (41) it can be seen that this velocity, w^*_{p0}, is given by

$$w^*_{\mathrm{p0}} = \tfrac{1}{2}(\tfrac{1}{2}h^*_0 - Bn)^2, \tag{55}$$

where $h_0^* = 1 + e\cos\theta^*$. For $\theta^* \ll 1$,

$$h_0^* = h_{00} + h_{01}\theta^{*2} + \ldots, \tag{56}$$

where

$$h_{00} = 1 + e, \quad h_{01} = -\tfrac{1}{2}e. \tag{57}$$

The solution in Region I is similar to that given earlier except that the location of the pseudo-yield surfaces will now be modified to

$$\bar{x} = \pm(Bn + B(\theta)). \tag{58}$$

$B(\theta)$ will be chosen so that the velocity on the pseudo-yield surface will no longer vary with θ. In Regions $\mathrm{I}_\pm$, then, we take the leading approximation to be

$$\tau_{xz} = -(\bar{x} \mp B(\theta)), \tag{59}$$

$$w_0 = -\tfrac{1}{2}[(\bar{x} \mp (Bn + B(\theta))^2 - (\tfrac{1}{2}h_0 - (Bn + B(\theta))^2]. \tag{60}$$

On the pseudo-yield surface the velocity takes the value w_{p0}, where

$$w_{p0} = \tfrac{1}{2}[(\tfrac{1}{2}h_0 - (Bn + B(\theta))]^2. \tag{61}$$

Region II is similar in some respects to that for $|\theta| > \theta^*$; in particular the first approximation to the velocity is independent of x. If it matches the true plug velocity on one side and w_{p0} on the other, it follows that $B(\theta)$ must be chosen such that $w_{p0} = w_{p0}^*$. This requires

$$B(\theta) = \tfrac{1}{2}(h_0 - h_0^*), \tag{62}$$

which for $|\theta| \ll 1$ becomes

$$B(\theta) = \tfrac{1}{2}h_{01}(\theta^2 - \theta^{*2}) + \ldots. \tag{63}$$

This requirement on $B(\theta)$ implies that the pseudo-yield surface runs parallel to the circular boundaries, precisely as would have been expected from the requirement that the velocity there is independent of θ.

The stress field in that part of Region II with $|\theta| < \theta^*$ is different from that for $|\theta| > \theta^*$, and a new solution of the momentum equation,

$$\frac{\partial \tau_{xz}}{\partial x} + \delta(1 + \delta x)^{-1}\left(\frac{\partial \tau_{\theta z}}{\partial \theta} + \tau_{xz}\right) = -1, \tag{64}$$

must be obtained. The proposed solution takes the form

$$\tau_{xz} = -C(\theta)\,\bar{x}, \tag{65}$$

where $C(\theta)$ is chosen so that $\tau_{xz} = \mp Bn$ at $\bar{x} = \pm(Bn + B(\theta))$, i.e.

$$C(\theta) = \frac{Bn}{Bn + B(\theta)}. \tag{66}$$

For $|\theta| \ll 1$ this reduces to

$$C(\theta) = 1 - \frac{1}{2Bn}h_{01}(\theta^2 - \theta^{*2}) + \ldots. \tag{67}$$

Substituting for τ_{xz} and $C(\theta)$ in (64) gives, to leading order in δ and θ,

$$\delta\frac{\partial \tau_{\theta z}}{\partial \theta} = -\frac{1}{2Bn}h_{01}(\theta^2 - \theta^{*2}) + \ldots. \tag{68}$$

A balance between these terms of apparently different orders of magnitude is achieved if θ is chosen to be $O(\delta^{\frac{1}{3}})$. On writing $\theta = \delta^{\frac{1}{3}}\phi$, $\theta^* = \delta^{\frac{1}{3}}\phi^*$ and integrating, this becomes

$$\tau_{\theta z} = -\frac{1}{2Bn} h_{01}(\tfrac{1}{3}\phi^3 - \phi^{*2}) + \dots, \tag{69}$$

where the constant of integration has been chosen so that $\tau_{\theta z} = 0$ at $\phi = 0$. The extent of the modified Region II (and hence of the true plug, Region III) is now determined by the requirement that $\tau_{\theta z} = -Bn$ at $\phi = \phi^*$, i.e.

$$\phi^* = \left(-\frac{3Bn^2}{h_{01}}\right)^{\frac{1}{2}}. \tag{70}$$

Note that $\tau_{\theta z} = Bn$ at $\phi = -\phi^*$ as required. In terms of e and θ^*, (70) becomes

$$\theta^* = \left(\frac{6Bn^2\delta}{e}\right)^{\frac{1}{3}}. \tag{71}$$

The yield surfaces are determined by the requirement that

$$\tau_{xz}^2 + \tau_{\theta z}^2 = Bn^2, \tag{72}$$

which gives, to leading order,

$$\bar{x}^2 + \left(\frac{e}{4Bn}\right)^2 (\tfrac{1}{3}\phi^3 - \phi^{*2}\phi)^2 = Bn^2. \tag{73}$$

We shall refer to the region within the yield surface as the true plug, even though strictly speaking we need to calculate the stress field in this region to confirm that yielding does not occur; this requires specification of the material properties at stresses below the yield stress and will not be examined in this paper. These results confirm that the true plug disappears for a Newtonian fluid, for which $Bn = 0$. For a Bingham plastic the extent of the true plug increases as the offset of centres decreases. When θ^* is $O(1)$, corresponding to $e \sim \delta$, the theory presented here breaks down and new scalings are required. This will not be investigated here, but we note that the growth of the true plug as e decreases is consistent with the fact that for a concentric annulus ($e = 0$) the true plug extends all round the annulus.

Similar remarks apply to the region near $\theta = \pi$ if Bn is sufficiently small for the pseudo-plug to extend all round the annulus. The inner edge of the pseudo-plug again runs parallel to the circular boundaries, but this time it narrows towards $\theta = \pi$. It can be shown that the solution is entirely analogous to that given above for the region near $\theta = 0$ and, in particular, that the azimuthal widths of the plugs are identical to leading order.

3.4. *Flow rate*

Finally, in this section, we demonstrate how the flow rate through the annulus depends upon Bn. If Q^* is the dimensional flow rate, then a dimensionless flow rate, Q, is defined by writing

$$Q^* = \frac{r_1 d^{*2}\tau_y}{Bn\mu_0^*} Q, \tag{74}$$

where

$$Q = 2\int_0^{\pi}\int_{-\frac{1}{2}h}^{\frac{1}{2}h} w(1+\delta\bar{x})\,\mathrm{d}\bar{x}\,\mathrm{d}\theta. \tag{75}$$

It has already been noted that under certain conditions the fluid will be motionless for $|\theta| > \theta_c$ and in these cases the upper limit of the first integral should be replaced by θ_c; in general the limit should be $\min(\pi, \theta_c)$.

A lowest-order approximation to the flow rate for small δ is

$$Q_0 = 2\int_0^{\min(\pi,\theta_c)} \int_{-\frac{1}{2}h_0}^{\frac{1}{2}h_0} w_0 \, d\bar{x} \, d\theta. \tag{76}$$

Using (40), (41) for w_0 it can be shown that

$$\int_{-\frac{1}{2}h_0}^{\frac{1}{2}h_0} w_0 \, dx = \frac{1}{12}(h_0^3 - 3Bnh_0^2 + 4Bn^3). \tag{77}$$

This is the classic expression for the flow rate of a Bingham Plastic in a slot of thickness h_0 (see, Bird *et al.* 1983). Using $h_0 = 1 + e\cos\theta$ and integrating over $(0, \min(\pi, \theta_c))$ gives

$$\begin{aligned} Q_0 = {} & \tfrac{1}{6}(1 - 3Bn + 4Bn^3)\,\theta_c + \tfrac{1}{2}e(1 - 2Bn)\sin\theta_c \\ & + \tfrac{1}{8}e^2(1 - Bn)(\sin 2\theta_c + 2\theta_c) + \tfrac{1}{6}e^3(\sin\theta_c - \tfrac{1}{3}\sin^3\theta_c). \end{aligned} \tag{78}$$

Here θ_c stands for $\min(\pi, \theta_c)$.

In the main body of the annulus the next approximation to w is $O(\delta)$ and this provides a similar correction to Q. The augmented solution near $\theta = 0, \pi$ provides a correction to w which is slightly larger, $O(\delta^{\frac{2}{3}})$, but it holds over a limited range in θ of width $O(\delta^{\frac{1}{3}})$. The effect is another correction $O(\delta)$ to the flow rate. It would not appear to be worthwhile, therefore, to evaluate the second correction without also evaluating the first. However, when the results of this theory are compared with our numerical results, there is much better agreement in the middle part of the annulus than might have been expected. It would seem, on this basis, that the largest numerical correction to Q_0 does, in fact, come from the augmented solution near $\theta = 0, \pi$ and, therefore, this correction will now be evaluated.

Near $\theta = 0$ the effective half-width of the plug is $Bn + B(\theta)$ with $B(\theta)$ defined as in (63). If this is substituted for Bn in (77), then the leading-order correction is

$$B(\theta)(Bn^2 - \tfrac{1}{4}(1 + e)^2). \tag{79}$$

Integrating with respect to θ over $-\theta^*$ to θ^* gives the correction, δQ, to the flow rate as

$$\delta Q = \tfrac{1}{3}e(Bn^2 - \tfrac{1}{4}(1 + e)^2)\,\theta^{*3}. \tag{80}$$

The simplest way of calculating the solution when the flow rate, Q^*, rather than the pressure gradient is specified is to use (74) to define Q in terms of Bn and then to solve the nonlinear algebraic equations (78), (80) for Bn.

3.5. *Discussion of the leading-order solution*

Except for those regions near the widest and narrowest sections of the annulus, the flow regime consists of a central pseudo-plug (Region II) of width $2Bn$, flanked by shearing regions (Regions $I_\pm$), as shown in figures 2, 3. This structure is similar to that for a slot of uniform thickness, the main difference being that the stress in the pseudo-plug is greater than the yield stress and that the velocity in the pseudo-plug is constant across it but not along it. True (unyielded) plugs exist at the widest (and also possibly the narrowest) parts of the annulus, their azimuthal extent depending essentially on the eccentricity, e, of the annulus.

If $Bn < \frac{1}{2}(1-e)$ then the pseudo-plug is narrower than the narrowest part of the annulus and therefore extends all the way round. In this case the structure of the solution near $\theta = \pi$ is similar to that near $\theta = 0$; in fact all that need be changed is the replacement of θ with $\pi - \theta$ in the leading-order solution.

If $Bn > \frac{1}{2}(1-e)$ there is a critical angle, θ_c, at which the thickness of the pseudo-plug is exactly equal to the gap thickness. To a first approximation θ_c is given by

$$\theta_c = \cos^{-1}\left(\frac{2Bn-1}{e}\right). \tag{81}$$

For $|\theta| < \theta_c$ the solution given above holds, but the fluid is motionless when $|\theta| > \theta_c$.

The two limiting cases in which Bn is close to $\frac{1}{2}(1-e)$ or $\frac{1}{2}(1+e)$ are of special interest because then the critical angle, θ_c, for the onset of the stationary segment is close to π and 0, respectively. First, suppose that Bn is close to $\frac{1}{2}(1-e)$ and write

$$Bn = \tfrac{1}{2}(1-e) + bn_1, \tag{82}$$

where bn_1 is small and positive. Then, substituting into (81) and expanding about $\frac{1}{2}(1-e)$ gives

$$\theta_c = \pi - \theta_1, \tag{83}$$

where

$$\theta_1 = (4bn_1/e)^{\frac{1}{2}}. \tag{84}$$

If $\theta_1 > \theta^*$ the solution is as given above. For $\theta_1 < \theta^*$, on the other hand, the true-plug region extends beyond the point where the stationary segment would have started. In this range of parameters the fluid flows on the narrow side, albeit slowly. The condition for the fluid to cease flowing altogether on the narrow side must now be modified to

$$Bn > \tfrac{1}{2}(1-e) + \tfrac{1}{4}e\left(\frac{3(1-e)^2\delta}{2e}\right)^{\frac{2}{3}} = Bn_1, \tag{85}$$

say.

Now suppose that Bn is so large that the pseudo-plug almost fills the gap on the wide side of the annulus, i.e.

$$Bn = \tfrac{1}{2}(1+e) - bn_2, \tag{86}$$

where, now, Bn_2 is small and positive. Then, substituting into (81) and expanding about $\frac{1}{2}(1+e)$ gives

$$\theta_c = (4bn_2/e)^{\frac{1}{2}}. \tag{87}$$

If $\theta_c > \theta^*$ then the solution is as given above, but with only a narrow sheared region between the stationary segment and the true plug near $\theta = 0$. For $\theta_c < \theta^*$, on the other hand, the true-plug region extends beyond the point where the stationary segment would have started. In this range of parameters the velocity of the true plug is zero and, consequently, there is no flow at all in the annulus. Thus, the condition for the fluid to be stationary throughout the annulus must be modified to

$$Bn > \tfrac{1}{2}(1+e) - \tfrac{1}{4}e\left(\frac{3(1+e)^2\delta}{2e}\right)^{\frac{2}{3}} = Bn_2, \tag{88}$$

say.

These results for the dependence of the flow pattern on Bn may be summarized as follows:

For $Bn < Bn_1$ true plug for $|\theta| < \theta^*$;
pseudo-plug for $\theta^* < |\theta| < \pi - \theta^*$;

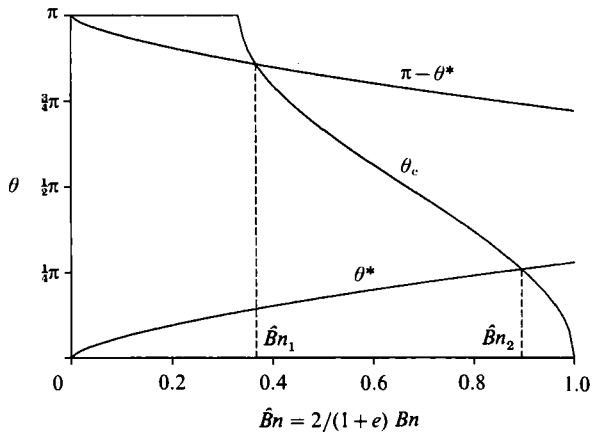

FIGURE 5. Critical angles for $\delta = 0.1$, $e = 0.5$.

	true plug for $\|\theta\| > \pi - \theta^*$.
For $Bn_1 < Bn < Bn_2$	true plug for $\|\theta\| < \theta^*$;
	pseudo-plug for $\theta^* < \|\theta\| < \theta_c$;
	stationary segment for $\|\theta\| > \theta_c$.
For $Bn > Bn_2$	no flow at all.

This division of flow regimes is illustrated in figure 5 for $\delta = 0.1$, $e = 0.5$.

4. Numerical solution

The only previous attempt at a numerical solution of the flow of a Bingham plastic in an eccentric annulus was by Guckes (1975), who used a finite-difference scheme. His results covered only a very restricted part of the parameter space owing to numerical difficulties associated with the loss of significant digits in regions of plug flow where the velocity gradients are zero and the viscosity is theoretically infinite. Other methods which have been considered for this calculation are boundary-element methods and spectral methods. Boundary-element methods are restricted to a limited class of problems and only recently have researchers attempted to solve nonlinear elliptic equations. Spectral methods could be applied to this problem, for the geometry lends itself to a Fourier expansion azimuthally which would lead to a system of ordinary differential equations in the radial direction. The ordinary differential equations would be solved as boundary-value problems, because of the no-slip conditions on the inner and outer cylinders, and so shooting or some equivalent scheme would be required. The success of the spectral method would depend on the ease with which the ordinary differential equations could be solved.

The most commonly used numerical schemes for flows such as these are based on finite-element techniques (O'Donovan & Tanner 1984; Gartling & Phan-Thien 1984; Crochet, Davis & Walters 1984; Beris *et al.* 1985). They are particularly suitable to complex geometries and have the additional advantage of remaining stable when large gradients occur in the interior of the domain. Nevertheless, it is necessary to exclude the possibility of the shear rate $\dot{\gamma}$ reducing exactly to zero for this would make the viscosity infinite. In (10) then, it is necessary to replace $\dot{\gamma}$ with $\dot{\gamma} + \epsilon$, where ϵ is a small number, typically about 10^{-8}. The finite-element method is then applied to this problem by using quadratic shape functions. Each element has eight nodes and an iso-parametric transformation allows elements to align themselves with the

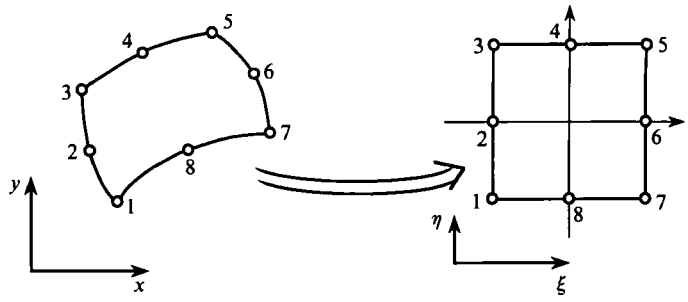

FIGURE 6. Parametric element mapping.

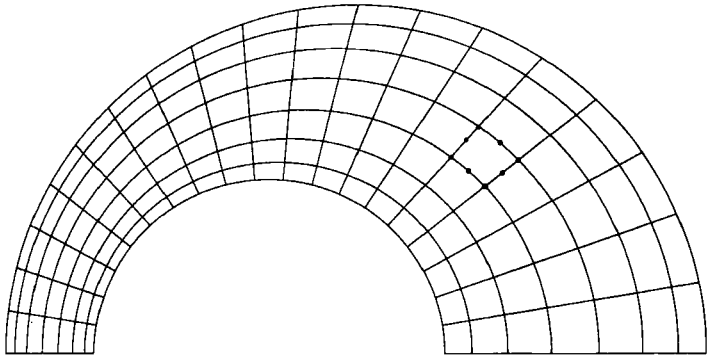

FIGURE 7. Finite-element mesh.

boundary. The notation used here closely follows that of the NAG Finite Element Library and the routines from that library were used in the computation. Let us write

$$x_1 = \sum_{i=1}^{8} N_i(\xi,\eta)\, x_{1i}, \tag{89}$$

$$x_2 = \sum_{i=1}^{8} N_i(\xi,\eta)\, x_{2i}, \tag{90}$$

where the curvilinear element in the (x_1, x_2)-plane has been mapped onto a square in the (ξ,η)-plane by the shape functions N_i. Here the points (x_{1i}, x_{2i}) are the nodal positions in the (x_1, x_2)-plane. The transformation is shown in figure 6 and the full finite-element mesh in figure 7. The shape functions in terms of (ξ,η)-coordinates are

$$N_i(\xi,\eta) = \tfrac{1}{4}(1+\xi\xi_i)(1+\eta\eta_i)(\xi\xi_i+\eta\eta_i-1), \tag{91}$$

at the corner nodes. For a typical mid-side node, e.g. $\xi_i = 0$, $\eta_i = 1$ the shape function is

$$N_i(\xi,\eta) = \tfrac{1}{2}(1-\xi^2)(1+\eta\eta_i). \tag{92}$$

Because of the iso-parametric representation the solution is of the form

$$w = \sum_{i=1}^{8} N_i(\xi,\eta)\, w_i \tag{93}$$

on each element. We now define the inner product

$$\langle f;g\rangle \equiv \iint_{\Omega} fg\,\mathrm{d}\Omega. \tag{94}$$

A weak form of the equation of motion is formed by multiplying the equation of motion by each shape function in turn and integrating over the cross-section. Thus for just one element

$$\langle N_i; \nabla \cdot (\mu \nabla w) \rangle = \langle N_i; P \rangle. \tag{95}$$

Writing $N_{i,x}$ for $\partial N_i/\partial x$ and using Green's theorem we obtain

$$\langle N_{i,x}; \mu w_{,x} \rangle + \langle N_{i,y}; \mu w_{,y} \rangle = -P \langle N_i; 1 \rangle, \tag{96}$$

where the boundary integrals have been ignored since they cancel on element–element edges. Substituting for w in this expression gives

$$(\langle N_{i,x}; \mu N_{j,x} \rangle + \langle N_{i,y}; \mu N_{j,y} \rangle) w_j = -P \langle N_i; 1 \rangle. \tag{97}$$

We note that μ is a function of w and so this gives a nonlinear system of equations. We can write the above as

$$M_{ij}(\mu(w))\, w_j = -P b_i, \tag{98}$$

showing explicitly the dependence of M on w. We can now linearize this equation by the Picard iteration

$$M_{ij}(\mu(w^{k-1}))\, w_j^k = -P b_i. \tag{99}$$

For a specified pressure gradient P is set equal to 1. For a specified flow rate P is determined by the constraint given by (15). We could have chosen to linearize the equation using Newton iteration, however the difficult nature of the viscosity for Bingham fluids reduces the circle of convergence so dramatically that Newton iteration generally fails.

A method for finding the unknown pressure gradient P is to write out the constraint equation as

$$\langle w; 1 \rangle = \langle 1; 1 \rangle, \tag{100}$$

which leads us to the extra algebraic equation

$$\sum_i \langle N_i; 1 \rangle w_i = \langle 1; 1 \rangle. \tag{101}$$

Thus, the solution is found by including this algebraic equation with the equation of motion and solving for

$$(w_1, \ldots, w_n | P)^{\mathrm{T}}, \tag{102}$$

where there are n nodes. The sparse matrix is a doubly bordered band diagonal matrix whose symmetry can be maintained since the inner product on the right-hand side of (97) is the same as the inner product on the left-hand side of (101). A special routine was written to solve this system of algebraic equations which was based on a banded solver published by the IMSL.

The construction of matrix $\boldsymbol{M}$ involves performing the integrals represented by the inner products in (97). We must also find the viscosity variation over each element and so the rate of strain. Substituting (93) into the non-dimensional form of (5) produces

$$\dot{\gamma} = \left[\left(\sum_i N_{i,x} w_i \right)^2 + \left(\sum_i N_{i,y} w_i \right)^2 \right]^{\frac{1}{2}}. \tag{103}$$

Equation (97) cannot be integrated explicitly, so solutions were obtained numerically using a nine-point Gaussian quadrature rule for each element. We shall not go into the full details of constructing $\boldsymbol{M}$ and just note that the band width of the main diagonal of $\boldsymbol{M}$ is determined by the ordering of the nodes on the finite-element mesh.

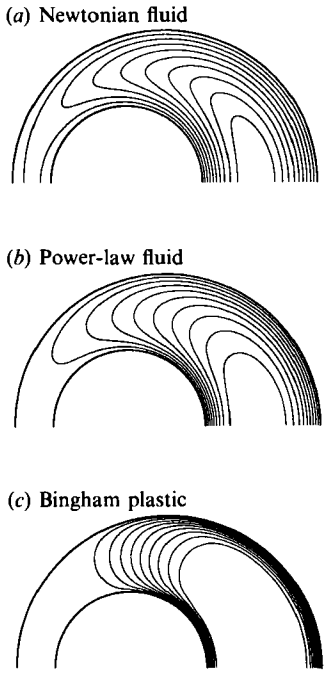

FIGURE 8. Velocity contours.

5. Results and conclusions

In order to gain some impression of the different flow patterns obtained with different fluids, numerical solutions have been obtained for three different fluids. Figure 8 shows contours of constant velocity in an annulus with a radius ratio of 0.5 and offset of 0.5. This radius has been chosen so that the contours can be seen clearly. Figure 8(*a*) shows a Newtonian fluid. For a fixed geometry the Newtonian solution is universal for the scalings used earlier. There are nine contours, equally spaced between zero and the peak velocity, which show that the flow is fastest through the wide side of the annulus and is proceeding more slowly through the narrow side. Figure 8(*b*) shows the flow of a power-law fluid of power index 0.5. Again nine equally spaced contours have been plotted. The fast-moving region of low shear on the wide side of the annulus has increased in extent, compared to the Newtonian result, and consequently the shear rates near the walls have been increased. Figure 8(*c*) shows nine contours for a Bingham plastic with the parameter Bn (now defined in terms of a given flow rate) set to 25. A large plug region exists on the wide side of the annulus with very high shear rates near the walls. From the contours we can deduce that the flow rate through the narrow side of the annulus must be very low. The next figures will quantify this effect.

Figure 9 shows four frames of the flow profiles in the narrowest and widest sections of the annulus for a power-law fluid of power index 0.5. The radius ratio in these calculations is 0.8 and for convenience the centrebody has not been drawn to scale in these results. Figure 9(*a*) shows a concentric annulus and since the velocity is scaled relative to the mean velocity the peak velocity is approximately 1.3. Figure 9(*b*) shows the effect of changing the offset to 0.25. The change in the flow profiles is dramatic, with rapid flow up the wide side of the annulus at over twice the mean velocity whilst the peak velocity on the narrow side of the annulus is reduced to less

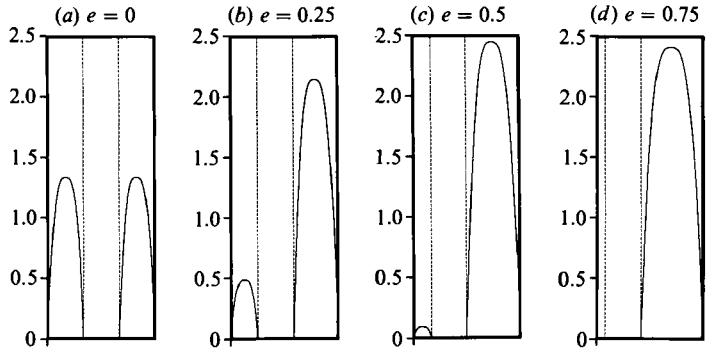

FIGURE 9. Typical radial velocity distribution for a power-law fluid.

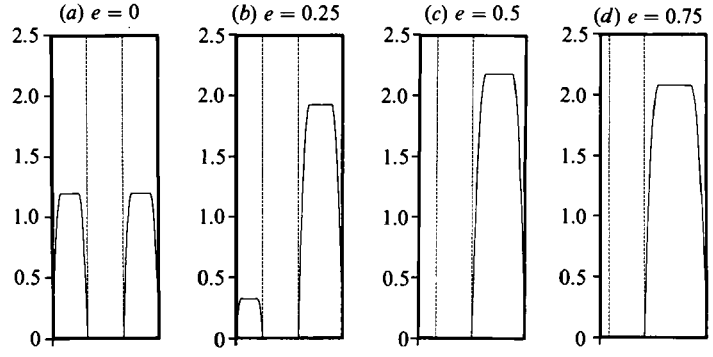

FIGURE 10. Typical radial velocity distribution for a Bingham plastic.

than half the mean velocity. Figure 9(*c*) shows an offset of 0.5 and the effect is accentuated further. Figure 9(*d*) shows an offset of 0.75 where there is now almost no flow up the narrow side. The peak velocity on the narrow side of the annulus is never identically zero since the fluid does not exhibit a yield stress.

Figure 10 shows four similar results but for a Bingham plastic with the parameter Bn set to 10. Figure 10(*a*) is for a concentric annulus and displays the characteristic flat profiles where the stress has fallen below the yield stress. Figure 10(*b*) is for an offset of 0.25 and shows a greater reduction in the narrow side velocity than was seen for the power-law fluid. Figure 10(*c*) for an offset of 0.5 indicates that the flow has stopped on the narrow side of the annulus. The final figure, 10(*d*), emphasizes this further. Also notice the wider plug on the wide side of the annulus in the final frame.

Figure 11 shows a plot of the centreline velocity as a function of angular position. The flow is of a Bingham fluid in an annulus with radius ratio 0.5 and offset 0.5 with the parameter Bn set to 10. The angular position is measured in radians and is zero in the widest part of the annulus and π in the narrowest part. The diagram shows that there is a true-plug region in the wide side of the annulus and a large immobile region in the narrow side.

In order to compare the numerical results with the narrow-gap asymptotic solution over a range of values of offset, e, Bingham Number, Bn, and dimensionless gap width, δ, it is first convenient to rescale Bn (defined now in terms of a given pressure gradient) by writing

$$Bn = \tfrac{1}{2}(1+e)\hat{B}n. \tag{104}$$

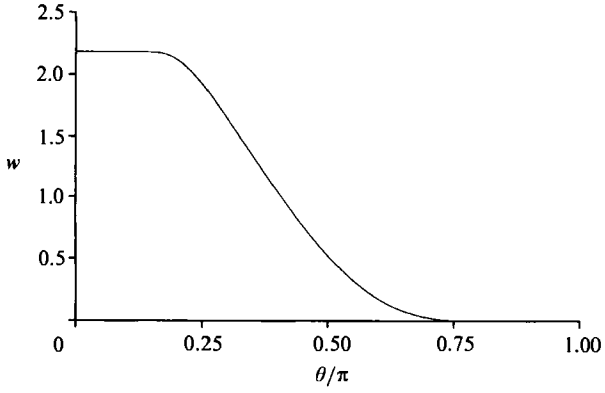

FIGURE 11. Typical azimuthal velocity distribution.

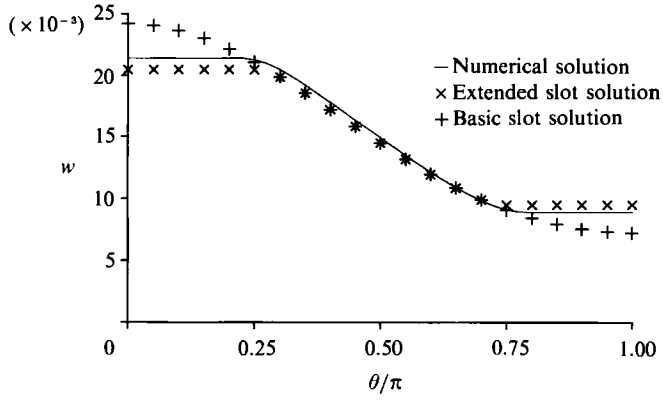

FIGURE 12. Centreline velocity for $\delta = 0.1$, $e = 0.1$, $\hat{B}n = 0.6$.

Then, whatever the value of e, $\hat{B}n$ ranges from 0 for a Newtonian fluid to 1 for a Bingham plastic for which the yield stress is so large that the pseudo-plug fills the gap on the wide side of the annulus.

An indication of the qualitative agreement on the structure of the solution and the accuracy that might be expected is obtained by examining the predictions for the variation of the velocity at the centreline of the annulus with azimuthal angle, θ. A sample result is shown in figure 12 for $\delta = 0.1$, $e = 0.1$ and scaled Bingham number, $\hat{B}n = 0.6$. Two analytic approximations are shown: a basic one, which excludes from consideration the true plugs near $\theta = 0, \pi$, and an extended one which includes the leading approximation in these regions. It can be seen from figure 12 that both approximations agree very well with the numerical results in the middle range of angles; in fact agreement is better than the 10% error that might be expected from these solutions with $\delta = 0.1$. The extended solution also performs very well in predicting the location of the true plugs and the velocity of the fluid within them. The basic analytic approximation cannot, of course, predict the location of the true plugs and its prediction of the velocities at the widest and narrowest parts of the annulus is in error by some 20%.

Comparisons of the numerical solution and approximate analytic solution have been made for a range of values of $\delta, e, \hat{B}n$. Results for $\delta = 0.1$ and $e = 0.5$ are shown

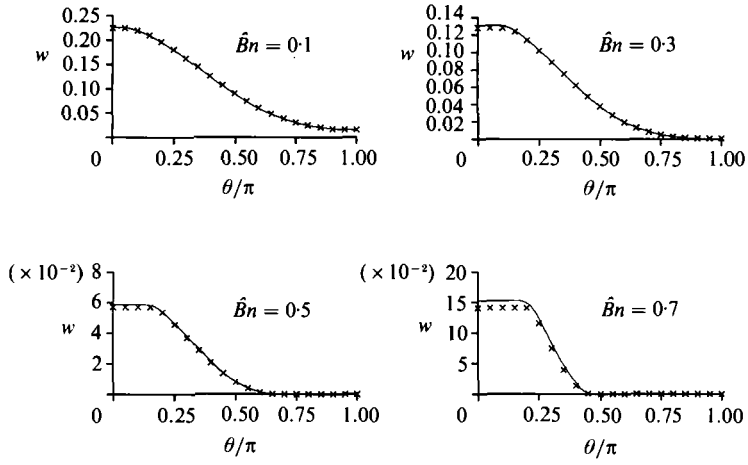

FIGURE 13. Centreline velocity for $\delta = 0.1$, $e = 0.5$: ——, numerical solution; ×, extended slot solution.

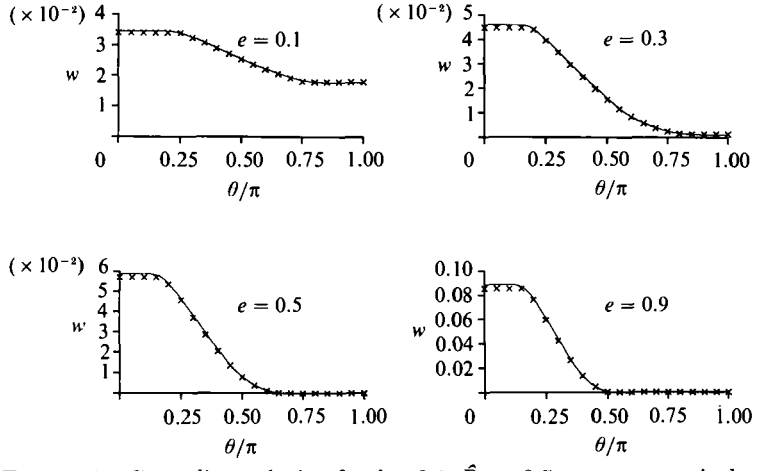

FIGURE 14. Centreline velocity for $\delta = 0.1$, $\hat{B}n = 0.5$: ——, numerical solution; ×, extended slot solution.

in figure 13. Agreement is excellent for values of the scaled Bingham number below about 0.7, but appears to deteriorate progressively beyond that. For these higher values of $\hat{B}n$ the transition between the true plug and stationary segment takes place over an ever narrowing range of angles, generating large gradients in the velocity and stress fields. Prediction of the plug velocity is in error by about 20% for $\hat{B}n = 0.85$, but this is largely a reflection of the steep variation of velocity with angle. No numerical solutions could be obtained for $\hat{B}n > 0.85$, which is consistent with the predictions of the extended slot model that there is no flow for $\hat{B}n > 0.87$ in this case. The basic analytic approximation predicts flow right up to $\hat{B}n = 1$.

Sample solutions for a range of offsets, e, with $\delta = 0.1$ and $\hat{B}n = 0.5$ are shown in figure 14. Once again agreement is excellent. The predicted narrowing of the true plugs as e increases is apparent.

A more severe test of the extended slot model is to compare it with the numerical results over a range of values of δ. Figure 15 shows such a comparison for $\hat{B}n = 0.5$

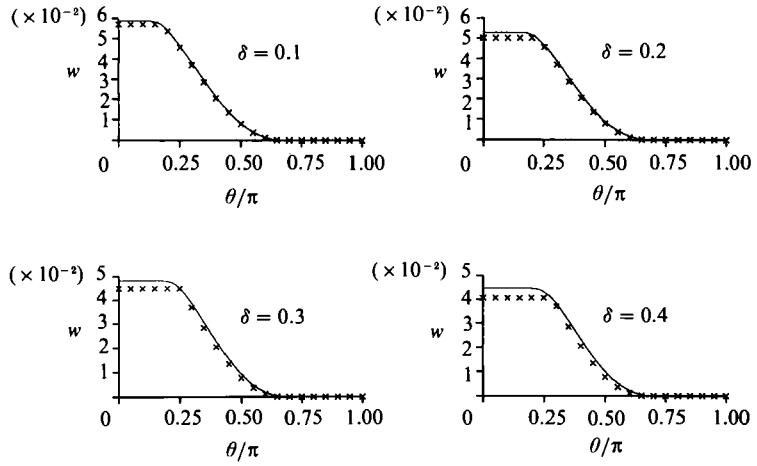

FIGURE 15. Centreline velocity for $e = 0.5$, $\hat{B}n = 0.5$: ——, numerical solution; ×, extended slot solution.

and $e = 0.5$. Excellent agreement is achieved for $\delta \leqslant 0.2$ and the error is still only about 10% for δ as high as 0.4. The extent of the stationary region is almost unaffected by changes in δ, but the true plug grows wider.

In summary, there is good qualitative and quantitative agreement between the numerical solutions and the asymptotic analytic solutions provided that the leading-order solution is determined throughout the entire flow field. In particular, the location and extent of various flow regions is confirmed. An important result is that the main part of the annulus contains regions that are plug-like in so far as the velocity is constant across the plug, but varies along it. The shear is zero in the radial direction but non-zero in the azimuthal direction, leading to a stress greater than the yield stress throughout this region. Close examination of the regions near the widest and narrowest sections of the annulus reveals that here true plugs do exist and that their shape and size is dependent on the eccentricity of the annulus. It would be premature to speculate on the significance of these results for the flow of Bingham plastics in other complex geometries, but it would be reasonable to expect that the regions that other authors have termed plugs are, strictly speaking, only pseudo-plugs. However, the possibility of the coexistence of true plugs with the pseudo-plugs cannot now be ruled out, although they might be of only finite extent and difficult to discover.

We wish to thank Ian Sobey for useful discussions during the early stages of this work and Sarah Weatherley for helping with the diagrams. We are grateful to a referee for pointing out to use the relevance of the theory of rigid/plastic solids.

REFERENCES

BERCOVIER, M. & ENGLEMAN, M. 1980 A finite element method for incompressible non-Newtonian flows. *J. Comput. Phys.* **36**, 313–326.

BERIS, A. N., TSAMOPOULOS, J. A., ARMSTRONG, R. C. & BROWN, R. A. 1985 Creeping motion of a sphere through a Bingham plastic. *J. Fluid Mech.* **158**, 219–244.

BIRD, R. B., DAI, G. C. & YARUSSO, B. J. 1983 The rheology and flow of viscoplastic materials. *Rev. Chem. Engng* **1**, 36–69.

CROCHET, M. J., DAVIES, A. R. & WALTERS, K. 1984 *Numerical Simulation of Non-Newtonian Flow.* Elsevier.

GARTLING, D. K. & PHAN-THIEN, N. 1984 A numerical simulation of a plastic fluid in a parallel-plate plastometer. *J. Non-Newtonian Fluid Mech.* **14**, 347–360.

GUCKES, T. L. 1975 Laminar flow of non-Newtonian fluid in an eccentric annulus. *Trans. ASME* B: *J. Engng Indust.* **97**, 498–506.

HILL, R. 1950 *The Mathematical Theory of Plasticity.* Oxford University Press.

IYOHO, A. W. & AZAR, J. J. 1980 An accurate slot flow model for non-Newtonian fluid flow through eccentric annuli. *Paper* SPE 9447 *Presented at the 55th Annual Technical Conf., Dallas.*

LIPSCOMBE, G. G. & DENN, M. M. 1984 Flow of Bingham fluids in complex geometries. *J. Non-Newtonian Fluid Mech.* **14**, 337–346.

MITSUISHI, N. & AOYAGI, Y. 1973 Non-Newtonian fluid flow in an eccentric annulus. *J. Chem. Engng Japan* **6**, 402–408.

O'DONOVAN, E. J. & TANNER, R. I. 1984 Numerical study of the Bingham squeeze film problem. *J. Non-Newtonian Fluid Mech.* **15**, 75–83.

SNYDER, W. T. & GOLDSTEIN, G. A. 1965 An analysis of fully developed flow in an eccentric annulus. *AIChEJ.* **11**, 462–467.